

A NEURAL NETWORK APPROACH FOR UNCERTAINTY QUANTIFICATION FOR TIME-DEPENDENT PROBLEMS WITH RANDOM PARAMETERS

TONG QIN , ZHEN CHEN , JONH JAKEMAN , AND DONGBIN XIU*

Abstract. In this work we propose a numerical framework for uncertainty quantification (UQ) for time-dependent problems with neural network surrogates. The new approach is based on approximating the exact time-integral form of the equation by neural networks, of which the structure is an adaptation of the residual network. The network is trained with data generated by running high-fidelity simulation or by conducting experimental measurements for a very short time. The whole procedure does not require any probability information from the random parameters and can be conducted offline. Once the distribution of the random parameters becomes available *a posteriori*, one can post-process the neural network surrogate to calculate the statistics of the solution. Several numerical examples are presented to demonstrate the procedure and performance of the proposed method.

Key words. Deep neural network, residual network, uncertainty quantification.

1. Introduction. Mathematical modeling is often subject to a wide range of uncertainties associated with parameter values, boundary/initial conditions, shape of domains etc. The quantification of the effects of such input uncertainty on the model outputs has attracted a significant amount of attention in the last two decades. Many methods have been developed to successfully deliver efficient and accurate uncertainty quantification (UQ). These include but not limited to the stochastic Galerkin methods [18, 52, 3], stochastic collocation methods [51, 2, 50], and Gaussian process regression methods [7, 8].

One challenge of UQ is that the dimension of the random parameter space is typically very high, which makes the traditional approximation approaches such as using polynomials suffer from the *curse of dimensionality* [5]. One remedy is to lessen this difficulty is to apply stochastic collocation methods on the *sparse-grid* [45]; see [51, 50, 32]. Besides the high-dimension approximation challenge, another challenge lies in dealing with the *epistemic uncertainty*. Most of the existing methods adopt probabilistic framework and model the uncertain inputs as random variables/processes and the probabilistic information of the input uncertainties is assumed, such as their probability distribution functions. However, in practice, such information is often missing or only partially known due to our lack of knowledge of the underlying physical systems. Such uncertainty, which is termed as *epistemic uncertainty*, has been discussed in many works, for example [21, 22, 16, 26, 12]. In particular, in [26, 12], the authors proposed methods that first estimate the range of the input uncertain parameters and then approximate the solution in this estimated parameter domain. The whole procedure does not require any probability information and the uncertainty quantification can be conducted as a post-processing step for the approximation of the solution.

On the other hand, recent years have seen explosive growth of research in machine learning, especially in the deep neural network (DNN). They have enjoyed great success in disciplines like image classifications [28], mastering Go game [44] and speech recognition [24], to name a few examples. For more thorough review of the latest

*Department of Mathematics, The Ohio State University, Columbus, OH 43210, USA. qin.428@osu.edu, chen.7168@osu.edu, jdjakeman@sandia.gov, xiu.16@osu.edu. Funding: This work was partially supported by AFOSR FA9550-18-1-0102.

development of DNNs, we refer the interested reader to a few relatively more recent review/summary type publications [34, 6, 15, 36, 14, 19, 42]. In addition to these aforementioned applications, efforts have also been devoted to apply DNN in various aspects of scientific computing. These include (but not limited to) the construction of reduced order model [23], aiding numerical solvers of conservation laws ([39, 40]), approximating the Koopman operator ([9]), solving and learning systems involving ODEs and PDEs [10, 31, 33, 11, 38, 49, 37, 41] etc.

The DNN enjoys two important theoretical properties: (i) it is a universal approximator [35, 4, 25], (ii) it can help lessen the curse of dimensionality [30]. These two properties make DNN well-suited for solving UQ problems. Several works [47, 54, 55, 53] have recently been done in this direction. In particular, in [47], the authors used DNNs as approximations for the mapping from the random parameter to the quantity of interest. Inspired by the active subspace surrogate [13], they proposed DNNs with the structure as a composition of a projection function and a link function. However, to generate the training data, it requires the distribution of the random inputs as well as full simulation to generate training data. In [54], the authors used the encoder-decoder neural network as the surrogate model and employed the Bayesian framework to accommodate the situation where the data is limited. This approach was further extended in [55] to the case where the data is unlabeled, i.e., without querying the numerical simulators. To this end, new loss functions were proposed, which are based on the residual norm [29] and variational form [48] of the PDEs. In another recent work [53], instead of replacing the input-output mapping with DNN, the authors approximated the distribution function of the solution directly. They train the neural networks in the adversarial inference framework and enforce the PDE-constraints by penalizing the loss function.

In this paper, we aim to employ DNNs to put forth a numerical framework for quantifying uncertainties of time-dependent problems, for which the cost of data acquisition, which usually involves long-time simulation, is high. Moreover, our framework does not require any *a priori* probabilistic information of the random parameters. In particular, we propose a DNN which approximates the exact time-integral form of the system. The resulting DNN is a generalization of the residual network which was first proposed in [20] for image analysis and was later applied in [37] to learn dynamical systems from data. To train the DNN, only very short-time simulations or experimental measurements with short time lags are required. The data generation and the network training require no probability knowledge of the random inputs. Only the ranges of the parameters are required, but they can be estimated with the approaches in [26, 12]. After the DNN is trained off-line, the UQ can be conducted as a post-processing step once the distribution of the random parameters becomes available *a posteriori*.

This paper is organized as follows. After the basic problem setup in Section 2, we present the main methods in Section 3 and some theoretical properties in Section 4. We then present, in Section 5, a set of numerical examples, covering both linear and nonlinear differential equations/systems, to demonstrate the effectiveness of the proposed algorithms.

2. Problem Setup. We are interested in studying the following differential system with random parameters.

$$\frac{d}{dt}\mathbf{x}(t, \boldsymbol{\alpha}(\omega)) = \mathbf{f}(\mathbf{x}, \boldsymbol{\alpha}(\omega)), \quad \mathbf{x}(0) = \mathbf{x}_0, \quad (2.1)$$

where $\mathbf{x} = (x_1, x_2, \dots, x_d) \in \mathbb{R}^d$ are state variables and $\boldsymbol{\alpha}(\omega) = (\alpha_1(\omega), \alpha_2(\omega), \dots, \alpha_l(\omega)) \in \mathbb{R}^l$ denotes the random parameters. Each component α_i of the random vector $\boldsymbol{\alpha}$ is assumed to be mutually independent of each other.

We assume that we are given the range of the random parameters. Otherwise, we can adopt the approach in [26] and [12] to get an estimated range with the probability that $\boldsymbol{\alpha}$ falls into the difference of the exact range and the estimated one smaller than a given small number $\eta > 0$. Let us use $I_{\boldsymbol{\alpha}} \subseteq \mathbb{R}^l$ to denote the (estimated) range of the parameters and we assume the problem (2.1) is well-posed for all $\boldsymbol{\alpha}$ in $I_{\boldsymbol{\alpha}}$.

We do not put any requirement on the distribution of the random parameters. The distribution can be given *a priori* or only becomes available *a posteriori*. The proposed method does not depend on any probability information of the random parameters.

The random effects of the input parameters will propagate along with time. The task of uncertainty quantification is to quantify the effects of the input uncertainty on the solution $\mathbf{x}(t)$ or on the quantity of interest $Q(\mathbf{x})$.

3. Methodology. In this section, we describe the main components of the proposed method.

3.1. Deterministic problem. Let us first consider the following system with deterministic parameters.

$$\begin{aligned} \frac{d}{dt}\mathbf{x}(t) &= \mathbf{f}(\mathbf{x}, \boldsymbol{\alpha}), \\ \mathbf{x}(0) &= \mathbf{x}_0. \end{aligned} \tag{3.1}$$

for $t \in [0, T]$ and $\boldsymbol{\alpha} \in I_{\boldsymbol{\alpha}}$. Assume that $I_{\mathbf{x}}$ is the domain of interest, such that $\mathbf{x}(t; \mathbf{x}_0, \boldsymbol{\alpha}) \in I_{\mathbf{x}}$ for $t \in [0, T]$ and $\boldsymbol{\alpha} \in I_{\boldsymbol{\alpha}}$.

This deterministic ODE (3.1) defines a mapping from the initial condition to the solution at $t = s$ as below

$$\mathbf{x}(s; \mathbf{x}_0, \boldsymbol{\alpha}) = \boldsymbol{\Phi}_s(\mathbf{x}_0; \boldsymbol{\alpha}), \quad \boldsymbol{\alpha} \in I_{\boldsymbol{\alpha}}, \quad s > 0.$$

We call this mapping the *flow map* for the ODE (3.1).

In practice, for each parameter configuration, high-fidelity simulations for solving are often too expensive to run for a long time. Or sometimes the equation itself (3.1) is unavailable and only measurements of the state variables for given parameters $\boldsymbol{\alpha}$ and time t are allowed. In both scenarios, one way to get around is to use short-time simulations or experiment measurements data to construct an approximate model.

More specific, let us use Δ to denote the maximum affordable simulation time or the time lag between two measurements. Then suppose that for each parameter sample $\boldsymbol{\alpha}_j \in I_{\boldsymbol{\alpha}}$, we run high-fidelity simulations or do experimental measurements to obtain a pair of data

$$\mathbf{X}_j = (\mathbf{x}_j + \epsilon_j^{(1)}, \boldsymbol{\alpha}_j, \delta_j), \quad \mathbf{Y}_j = \boldsymbol{\Phi}_{\delta_j}(\mathbf{x}_j; \boldsymbol{\alpha}_j) + \epsilon_j^{(2)}$$

where $\delta_j \in I_{\Delta} = (0, \Delta]$ denotes the length of the simulation time or the time lag between two experiment measurements, and $\epsilon_j^{(1)}$ and $\epsilon_j^{(2)}$ denotes the potential measurement/simulation errors.

We use

$$S = \{(\mathbf{X}_j, \mathbf{Y}_j) : j = 1, \dots, J\} \tag{3.2}$$

to denote the set of training data. With these data pairs, we can obtain via the supervised learning an approximation for the flow map

$$\widehat{\Phi}_\delta(\mathbf{z}, \boldsymbol{\alpha}; \Theta) \approx \Phi_\delta(\mathbf{z}; \boldsymbol{\alpha}), \quad \forall (\mathbf{z}, \delta, \boldsymbol{\alpha}) \in I_{\mathbf{x}} \times I_\Delta \times I_\alpha, \quad (3.3)$$

where the set Θ includes all the model parameters which depends on the training data S . The construction of this approximation will be introduced in Section 3.2.

To obtain approximations for any $t \in [0, T]$, first note that, for autonomous systems, the flow map satisfies the following composition property

$$\Phi_{t+s} = \Phi_t \circ \Phi_s, \quad \forall t, s \geq 0. \quad (3.4)$$

Then, for any given $t \in [0, T]$, we decompose t into a summation of short time lags

$$t = \sum_{i=1}^n \delta_i, \quad \delta_i \in I_\Delta.$$

By (3.4), we have

$$\mathbf{x}(t; \mathbf{x}_0, \boldsymbol{\alpha}) = \Phi_{\delta_n} \circ \Phi_{\delta_{n-1}} \circ \Phi_{\delta_{n-2}} \circ \cdots \circ \Phi_{\delta_1}(\mathbf{x}_0; \boldsymbol{\alpha}), \quad (3.5)$$

which can be approximated by

$$\widehat{\mathbf{x}}(t; \mathbf{x}_0, \boldsymbol{\alpha}) = \widehat{\Phi}_{\delta_n} \circ \widehat{\Phi}_{\delta_{n-1}} \circ \widehat{\Phi}_{\delta_{n-2}} \circ \cdots \circ \widehat{\Phi}_{\delta_1}(\mathbf{x}_0, \boldsymbol{\alpha}; \Theta). \quad (3.6)$$

Now, the problem is reduced to how to obtain the flow map approximations $\widehat{\Phi}_\delta(\mathbf{z}, \boldsymbol{\alpha}; \Theta)$ for small time lags $\delta \in I_\Delta$ with the training data S .

3.2. Neural network approximation. One traditional way to approximate flow map $\widehat{\Phi}_\delta$ to use polynomials and fit the coefficients with the least-square approach. However, for UQ problems, the dimension of the parameter space is typically very high and polynomial approximation will suffer from the curse of dimensionality [5]. Alternatively, we employ the DNN to approximate the flow map. As oppose to the polynomial approximation, the DNN was recently shown to be able to lessen the dependence on dimension, especially when it gets deep [30].

3.2.1. Fully-connected neural network. The proposed DNN is based on fully connected feedforward neural network (FNN) with $M \geq 2$ hidden layers. The FNN can be represented as compositions of a sequence of activation functions and linear transformations

$$\mathbf{N}(\cdot; \Theta) = (\sigma_m \circ \mathbf{W}_m) \circ \cdots \circ (\sigma_2 \circ \mathbf{W}_1),$$

where \circ stands for operator composition, \mathbf{W}_j denotes the weight matrix, which is augmented with biases, for transforming the output of the j -th layer to the input of the $(j+1)$ -th layer, and $\sigma_j : \mathbb{R} \rightarrow \mathbb{R}$ is the activation function, which is applied component-wise to the inputs of the j -th layer. The weight matrices $\{\mathbf{W}_j\}_{j=1}^m$ are the model parameters. We use Θ to represent them.

3.2.2. Flow map approximation. For a given time lag $\delta \in I_\Delta$, if we integrate (3.1) from $t = 0$ to $t = \delta$, we have

$$\mathbf{x}(\delta; \mathbf{x}_0, \boldsymbol{\alpha}) = \mathbf{x}_0 + \int_0^\delta \mathbf{f}(\mathbf{x}(s), \boldsymbol{\alpha}) ds = \mathbf{x}_0 + \int_0^\delta \mathbf{f}(\Phi_s(\mathbf{x}_0; \boldsymbol{\alpha}), \boldsymbol{\alpha}) ds \quad (3.7)$$

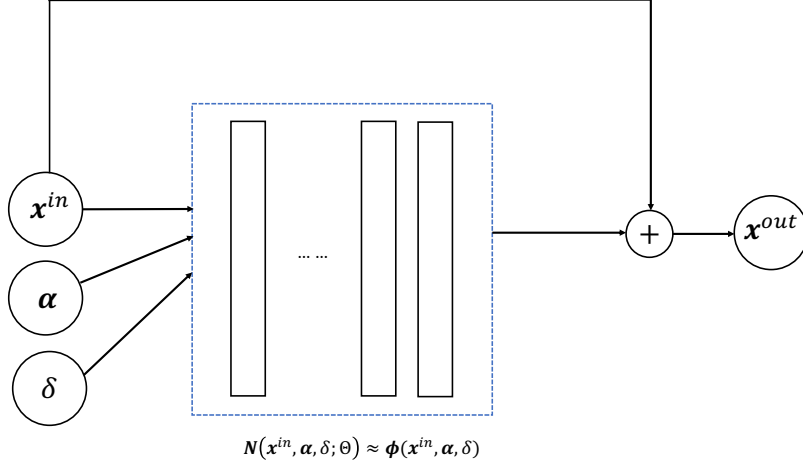


Fig. 3.1: Structure of the neural network.

If we define the effective increment over time lag δ

$$\phi(\mathbf{z}, \alpha, \delta) = \int_0^\delta \mathbf{f}(\Phi_\tau(\mathbf{z}; \alpha), \alpha) d\tau,$$

then by(3.7), the flow map Φ_δ can be rewritten as

$$\Phi_\delta(\mathbf{z}; \alpha) = \mathbf{z} + \phi(\mathbf{z}, \alpha, \delta),$$

for $(\mathbf{z}, \alpha, \delta) \in I_{\mathbf{x}} \times I_{\alpha} \times I_{\Delta}$. We remark that this is an exact representation for the flow map, which is valid for any $\Delta > 0$.

In general, the analytical form of the increment is unknown. We use FNN to approximate the effective increment $\phi(\mathbf{z}, \alpha, \delta)$ and define the approximate flow map

$$\widehat{\Phi}_\delta(\mathbf{z}, \alpha; \Theta) = \mathbf{z} + \mathbf{N}(\mathbf{z}, \alpha, \delta; \Theta), \quad (3.8)$$

where $\mathbf{N}(\cdot, \cdot, \cdot; \Theta)$ represents a fully connected neural network with parameter set Θ . The resulting network is a modification to the residual network (*ResNet*), which was first introduced in [20] and was later applied to learn governing equations in [37].

The main difference between the network employed here and the one that was used in [37] is that in addition to the state variable \mathbf{z} , we further allow the parameters α and time-lag δ to be training features. In Fig. 3.1, we show a schematic plot to illustrate the structure of the proposed network which is used to approximate the one-step flow map.

The parameters Θ can be trained by minimizing certain loss function on the training data S . We omit the details here and postpone it to the Section 5.

3.2.3. Uncertainty quantification. After the network get trained, we can use the approximate flow map $\widehat{\Phi}_\delta(\mathbf{z}, \alpha; \Theta)$ with $\delta \in I_{\Delta}$ to generate the approximation

$\widehat{\mathbf{x}}(t; \mathbf{z}, \boldsymbol{\alpha})$ as in (3.6). Then, we can use the model $\widehat{\mathbf{x}}(t; \mathbf{x}_0, \boldsymbol{\alpha})$ as an accurate surrogate of the solution $\mathbf{x}(t; \mathbf{x}_0, \boldsymbol{\alpha})$ for any given initial condition $\mathbf{x}_0 \in I_{\mathbf{x}}$ and parameter $\boldsymbol{\alpha} \in I_{\boldsymbol{\alpha}}$. Suppose the distribution of the random vector $\boldsymbol{\alpha}(\omega)$ is $\rho_{\boldsymbol{\alpha}}(s) = dF_{\boldsymbol{\alpha}}(s)/ds$, which is given or only becomes available after the surrogate model gets trained. We can evaluate various statistics of the solution $\mathbf{x}(t; \mathbf{x}_0, \boldsymbol{\alpha})$ by post-processing the solution surrogate.

For example, the mean and variance of the solution can now be approximated with

$$\begin{aligned} \mathbb{E}_{\boldsymbol{\alpha}}[\mathbf{x}(t; \mathbf{x}_0, \boldsymbol{\alpha})] &\approx \mathbb{E}_{\boldsymbol{\alpha}}[\widehat{\mathbf{x}}(t; \mathbf{x}_0, \boldsymbol{\alpha})] = \int_{I_{\boldsymbol{\alpha}}} \widehat{\mathbf{x}}(t; \mathbf{x}_0, \mathbf{y}) \rho_{\boldsymbol{\alpha}}(\mathbf{y}) d\mathbf{y}, \\ \text{Var}_{\boldsymbol{\alpha}}[\mathbf{x}(t; \mathbf{x}_0, \boldsymbol{\alpha})] &\approx \text{Var}_{\boldsymbol{\alpha}}[\widehat{\mathbf{x}}(t; \mathbf{x}_0, \boldsymbol{\alpha})] \\ &= \int_{I_{\boldsymbol{\alpha}}} [\widehat{\mathbf{x}}(t; \mathbf{x}_0, \mathbf{y}) - \mathbb{E}_{\boldsymbol{\alpha}}[\widehat{\mathbf{x}}(t; \mathbf{x}_0, \mathbf{y})]]^2 \rho_{\boldsymbol{\alpha}}(\mathbf{y}) d\mathbf{y}. \end{aligned} \quad (3.9)$$

The integrals in terms of $\widehat{\mathbf{x}}$ can be further approximated with quadrature or Monte Carlo methods.

3.3. Algorithm summary. The algorithm can be summarized as below.

1. Identify the domains $I_{\mathbf{x}}$, $I_{\boldsymbol{\alpha}}$ for the state variables and the parameters, respectively.
2. Draw J samples $\{(\mathbf{x}_j, \boldsymbol{\alpha}_j, \delta_j)\}_{j=1}^J$ from the domain $I_{\mathbf{x}} \times I_{\boldsymbol{\alpha}} \times I_{\Delta}$.
3. For each sample $(\mathbf{x}_j, \boldsymbol{\alpha}_j, \delta_j)$, use \mathbf{x}_j as the initial condition, $\boldsymbol{\alpha}_j$ as the parameter and solve the model (2.1) with any high-fidelity solver till $t = \delta_j$ and obtain \mathbf{Y}_j .
4. Train the neural network with $\{(\mathbf{x}_j, \boldsymbol{\alpha}_j, \delta_j)\}_{j=1}^J$ as the features and $\{\mathbf{Y}_j\}_{j=1}^J$ as the targets.
5. Post-process the neural network $\widehat{\boldsymbol{\Phi}}_{\delta}(\mathbf{z}, \boldsymbol{\alpha}; \Theta)$. It can be used as a surrogate to do predictions for a given deterministic parameter $\boldsymbol{\alpha} \in I_{\boldsymbol{\alpha}}$ or to do uncertainty quantification if the distribution of $\boldsymbol{\alpha}(\omega)$ becomes available.

4. Theoretical properties. In this section, we give some analysis to the proposed methods. First, we recall the classical universal approximation result for the neural network [35, Theorem 3.1].

PROPOSITION 4.1. *For any given function $f \in C(\mathbb{R}^d)$ and positive real number $\epsilon > 0$, there exists a single-layer neural network $N(\cdot; \Theta)$ with parameter Θ such that*

$$\max_{\mathbf{x} \in D} |f(\mathbf{x}) - N(\mathbf{x}; \Theta)| < \epsilon$$

for any compact set $D \in \mathbb{R}^n$, if and only if the activation functions are continuous and are not polynomials.

Given this universal approximation result, we have the following approximation result.

LEMMA 4.2. *Suppose the right hand side function $\mathbf{f}(\mathbf{x}, \boldsymbol{\alpha})$ in (2.1), is Lipschitz continuous with respect to the state variable with uniform Lipschitz constant L for all $\boldsymbol{\alpha} \in I_{\boldsymbol{\alpha}}$. If the neural network get well trained such that for a given small number $\mathcal{E} > 0$,*

$$|\mathbf{N}(\mathbf{z}, \boldsymbol{\alpha}, \delta; \Theta) - \boldsymbol{\phi}(\mathbf{z}, \boldsymbol{\alpha}, \delta)| \leq \mathcal{E}, \quad \forall (\mathbf{z}, \boldsymbol{\alpha}, \delta) \in I_{\mathbf{x}} \times I_{\boldsymbol{\alpha}} \times I_{\Delta}, \quad (4.1)$$

then we have

$$\|\widehat{\mathbf{x}}(t; \cdot, \cdot) - \mathbf{x}(t; \cdot, \cdot)\|_{L^{\infty}(I_{\mathbf{x}} \times I_{\boldsymbol{\alpha}})} \leq \frac{e^{nL\Delta} - 1}{e^{L\Delta} - 1} \mathcal{E}, \quad (4.2)$$

where $\mathbf{x}(t; \mathbf{z}, \boldsymbol{\alpha})$ and $\widehat{\mathbf{x}}(t; \mathbf{z}, \boldsymbol{\alpha})$ are as defined in (3.5) and (3.6) and $t = \sum_{i=1}^n \delta_i$.

REMARK 4.1. From the estimate (4.2), we observe that the error depends on the training loss \mathcal{E} and the number of compositions n . In particular, the error grows with n . In practice, for a given target time $t \in [0, T]$, we would like to take each time step as large as possible, i.e., $\delta_i = \Delta$. And only take a different size for the very last step.

Proof. First, for any $\mathbf{u}, \mathbf{v} \in I_{\mathbf{x}}$, and $(\boldsymbol{\alpha}, \delta) \in I_{\boldsymbol{\alpha}} \times I_{\Delta}$, let us consider

$$\begin{aligned} \left| \Phi_{\delta}(\mathbf{u}, \boldsymbol{\alpha}) - \widehat{\Phi}_{\delta}(\mathbf{v}, \boldsymbol{\alpha}; \Theta) \right| &\leq \left| \Phi_{\delta}(\mathbf{u}, \boldsymbol{\alpha}) - \Phi_{\delta}(\mathbf{v}, \boldsymbol{\alpha}) \right| + \left| \Phi_{\delta}(\mathbf{v}, \boldsymbol{\alpha}) - \widehat{\Phi}_{\delta}(\mathbf{v}, \boldsymbol{\alpha}; \Theta) \right| \\ &= \left| \Phi_{\delta}(\mathbf{u}, \boldsymbol{\alpha}) - \Phi_{\delta}(\mathbf{v}, \boldsymbol{\alpha}) \right| + \left| \phi(\mathbf{v}, \boldsymbol{\alpha}, \delta) - \mathbf{N}(\mathbf{v}, \boldsymbol{\alpha}, \delta; \Theta) \right| \\ &\leq e^{L\delta} \|\mathbf{u} - \mathbf{v}\| + \mathcal{E} \end{aligned}$$

where in the last step we have used (4.1) and the classical result on the continuity of dynamical system with respect to the initial data; see [46, p. 109].

Then for any given $t \in [0, T]$, and any decomposition $t = \sum_{i=1}^n \delta_i$ with $\delta_i \in I_{\Delta}$, we have

$$\begin{aligned} &\left| \widehat{\mathbf{x}}(t; \mathbf{z}, \boldsymbol{\alpha}) - \mathbf{x}(t; \mathbf{z}, \boldsymbol{\alpha}) \right| \\ &= \left| \widehat{\Phi}_{\delta_n} \circ \widehat{\Phi}_{\delta_{n-1}} \circ \dots \circ \widehat{\Phi}_{\delta_1}(\mathbf{z}, \boldsymbol{\alpha}; \Theta) - \Phi_{\delta_n} \circ \Phi_{\delta_{n-1}} \circ \dots \circ \Phi_{\delta_1}(\mathbf{z}; \boldsymbol{\alpha}) \right| \\ &\leq \mathcal{E} + e^{L\delta_n} \left| \widehat{\Phi}_{\delta_{n-1}} \circ \dots \circ \widehat{\Phi}_{\delta_1}(\mathbf{z}, \boldsymbol{\alpha}; \Theta) - \Phi_{\delta_{n-1}} \circ \dots \circ \Phi_{\delta_1}(\mathbf{z}; \boldsymbol{\alpha}) \right| \\ &\leq \mathcal{E} + e^{L\delta_n} \left[\mathcal{E} + e^{L\delta_{n-1}} \left| \widehat{\Phi}_{\delta_{n-2}} \circ \dots \circ \widehat{\Phi}_{\delta_1}(\mathbf{z}, \boldsymbol{\alpha}; \Theta) - \Phi_{\delta_{n-2}} \circ \dots \circ \Phi_{\delta_1}(\mathbf{z}; \boldsymbol{\alpha}) \right| \right] \\ &\leq \dots \\ &\leq \mathcal{E} \left(1 + e^{L\delta_n} + e^{L(\delta_n + \delta_{n-1})} + \dots + e^{L \sum_{i=2}^n \delta_i} \right) \\ &\leq \mathcal{E} \left(1 + e^{L\Delta} + e^{2L\Delta} + \dots + e^{(n-1)L\Delta} \right) \\ &= \frac{e^{nL\Delta} - 1}{e^{L\Delta} - 1} \mathcal{E} \end{aligned}$$

for any $(\boldsymbol{\alpha}, \mathbf{z}) \in I_{\boldsymbol{\alpha}} \times I_{\mathbf{x}}$. This implies the result (4.2). \square

For the approximation of the mean and variance, we have the following error estimates.

THEOREM 4.3. Under the same assumptions of Lemma 4.2 and assume the solution is bounded $\|\mathbf{x}(t; \cdot, \cdot)\|_{L^\infty(I_{\mathbf{x}} \times I_{\boldsymbol{\alpha}})} = C_t < \infty$. Then we have the following error estimate for the approximation of mean and variance

$$\left| \mathbb{E}_{\boldsymbol{\alpha}}[\mathbf{x}(t; \mathbf{x}_0, \boldsymbol{\alpha})] - \mathbb{E}_{\boldsymbol{\alpha}}[\widehat{\mathbf{x}}(t; \mathbf{x}_0, \boldsymbol{\alpha})] \right| \leq C(n, L, \Delta) \mathcal{E}, \quad (4.3)$$

$$\left| \text{Var}_{\boldsymbol{\alpha}}[\mathbf{x}(t; \mathbf{x}_0, \boldsymbol{\alpha})] - \text{Var}_{\boldsymbol{\alpha}}[\widehat{\mathbf{x}}(t; \mathbf{x}_0, \boldsymbol{\alpha})] \right| \leq 2C(n, L, \Delta)^2 \mathcal{E}^2 + 4C(n, L, \Delta) C_t \mathcal{E}, \quad (4.4)$$

where $C(n, L, \Delta) = \frac{e^{nL\Delta} - 1}{e^{L\Delta} - 1}$.

Proof. For the mean approximation (4.3), by Lemma 4.2, we have

$$\left| \mathbb{E}_{\boldsymbol{\alpha}}[\mathbf{x}(t; \mathbf{x}_0, \boldsymbol{\alpha})] - \mathbb{E}_{\boldsymbol{\alpha}}[\widehat{\mathbf{x}}(t; \mathbf{x}_0, \boldsymbol{\alpha})] \right| \leq \mathbb{E}_{\boldsymbol{\alpha}}[\|\mathbf{x}(t; \mathbf{x}_0, \boldsymbol{\alpha}) - \widehat{\mathbf{x}}(t; \mathbf{x}_0, \boldsymbol{\alpha})\|] \leq \frac{e^{nL\Delta} - 1}{e^{L\Delta} - 1} \mathcal{E}.$$

For the variance approximation, we have

$$\begin{aligned}
& |\text{Var}_\alpha[\mathbf{x}(t; \mathbf{x}_0, \boldsymbol{\alpha})] - \text{Var}_\alpha[\widehat{\mathbf{x}}(t; \mathbf{x}_0, \boldsymbol{\alpha})]| \\
&= |\mathbb{E}_\alpha[\mathbf{x}(t; \mathbf{x}_0, \boldsymbol{\alpha})^2] - \mathbb{E}_\alpha[\mathbf{x}(t; \mathbf{x}_0, \boldsymbol{\alpha})]^2 - \mathbb{E}_\alpha[\widehat{\mathbf{x}}(t; \mathbf{x}_0, \boldsymbol{\alpha})^2] + \mathbb{E}_\alpha[\widehat{\mathbf{x}}(t; \mathbf{x}_0, \boldsymbol{\alpha})]^2| \\
&\leq |\mathbb{E}_\alpha[\mathbf{x}(t; \mathbf{x}_0, \boldsymbol{\alpha})^2] - \mathbb{E}_\alpha[\widehat{\mathbf{x}}(t; \mathbf{x}_0, \boldsymbol{\alpha})^2]| + |\mathbb{E}_\alpha[\mathbf{x}(t; \mathbf{x}_0, \boldsymbol{\alpha})]^2 - \mathbb{E}_\alpha[\widehat{\mathbf{x}}(t; \mathbf{x}_0, \boldsymbol{\alpha})]^2| \\
&= \mathbb{E}_\alpha[|\mathbf{x}(t; \mathbf{x}_0, \boldsymbol{\alpha}) - \widehat{\mathbf{x}}(t; \mathbf{x}_0, \boldsymbol{\alpha})| |\mathbf{x}(t; \mathbf{x}_0, \boldsymbol{\alpha}) + \widehat{\mathbf{x}}(t; \mathbf{x}_0, \boldsymbol{\alpha})|] \\
&\quad + \mathbb{E}_\alpha[|\mathbf{x}(t; \mathbf{x}_0, \boldsymbol{\alpha}) - \widehat{\mathbf{x}}(t; \mathbf{x}_0, \boldsymbol{\alpha})|] \mathbb{E}_\alpha[|\mathbf{x}(t; \mathbf{x}_0, \boldsymbol{\alpha}) + \widehat{\mathbf{x}}(t; \mathbf{x}_0, \boldsymbol{\alpha})|] \\
&\leq 2 \frac{(e^{nL\Delta} - 1)\mathcal{E}}{e^{L\Delta} - 1} \mathbb{E}_\alpha[|\mathbf{x}(t; \mathbf{x}_0, \boldsymbol{\alpha}) + \widehat{\mathbf{x}}(t; \mathbf{x}_0, \boldsymbol{\alpha})|] \\
&\leq 2 \frac{(e^{nL\Delta} - 1)\mathcal{E}}{e^{L\Delta} - 1} (\mathbb{E}_\alpha[|\widehat{\mathbf{x}}(t; \mathbf{x}_0, \boldsymbol{\alpha}) - \mathbf{x}(t; \mathbf{x}_0, \boldsymbol{\alpha})|] + \mathbb{E}_\alpha[|2\mathbf{x}(t; \mathbf{x}_0, \boldsymbol{\alpha})|]) \\
&\leq 2 \frac{(e^{nL\Delta} - 1)^2}{(e^{L\Delta} - 1)^2} \mathcal{E}^2 + 4 \frac{(e^{nL\Delta} - 1)C_t}{e^{L\Delta} - 1} \mathcal{E}
\end{aligned}$$

This gives the result (4.4). \square

5. Numerical Examples. In this section we present numerical examples to verify the performance and properties of the proposed methods. In all the examples, we take $\Delta = 0.1$. The parameter domain I_α varies for different examples. The training data are generated by solving the ODEs with standard Runge-Kutta solvers with small time step size. The DNNs are trained by minimizing the mean square loss function

$$L(\Theta; \mathbf{X}, \mathbf{Y}) = \frac{1}{J} \sum_{j=1}^J \left| \widehat{\Phi}_{\delta_j}(\mathbf{x}_j, \boldsymbol{\alpha}_j; \Theta) - \mathbf{Y}_j \right|_2^2,$$

on the training data $\mathbf{X} = \{(\mathbf{x}_j, \boldsymbol{\alpha}_j, \delta_j)\}_{j=1}^J$ and $\mathbf{Y} = \{\mathbf{Y}_j\}_{j=1}^J$, by using the Adam algorithm [27] with the standard parameters.

In each example, we use the tuple (m, u) to denote the structure of \mathbf{N} , where m denotes the number of hidden layers and u denotes the number of nodes in each layer. The activation function is chosen as $\sigma = \tanh(x)$. For the size of training set, we take 20 times as many data pairs as the number of model parameters. All the networks are generated and trained with the open-source Tensorflow library [1]. The training data set is divided into mini-batches of size 30. And we typically train the model for 2000 epochs and reshuffle the training data in each epoch. All the weights are initialized randomly from Gaussian distributions and all the biases are initialized to be zeros.

After the approximation for the flow map $\widehat{\Phi}_\delta$ gets trained satisfactorily, we post-process it to compute the statistics of the solution as in (3.9) according to the distributions which are assigned *a posteriori*. When marching forward in time, in all the examples we simply take uniform step size $\delta_i = \Delta$ and march forward for n steps to illustrate the performance of the method.

Example 1: Linear Scalar ODE. Let us first consider the following linear ODE with a single random parameter

$$\frac{dx}{dt} = -\alpha(\omega)x, \quad x(0) = x_0, \quad (5.1)$$

where $\alpha(\omega)$ is a random coefficient. We take $I_\alpha = [0, 1]$ and $I_x = [0, 1]$. This simple stochastic equation has the following analytical solution

$$x(t; \alpha) = x_0 e^{-\alpha t}.$$

If $\alpha(\omega)$ is uniformly distributed in the interval $[0, 1]$, we have the exact mean of the solution

$$\mathbb{E}_\alpha[x(t; \alpha)] = \int_0^1 e^{-\alpha t} d\alpha = \frac{1 - e^{-t}}{t},$$

and the variance of it

$$\text{Var}_\alpha[x(t; \alpha)] = \frac{1 - e^{-2t}}{2t} - \left(\frac{1 - e^{-t}}{t} \right)^2. \quad (5.2)$$

We approximate the flow map with DNN of structure (3, 40). After the network get trained, the mean and variance are further computed by applying a ten-point Gaussian quadrature over the parameter interval I_α to approximate the integrals in (3.9). In Fig. 5.1, we show the results after marching forward for 300 steps with $x_0 = 1$. The results are comparable with the results obtained by the time-dependent gPC in [17].

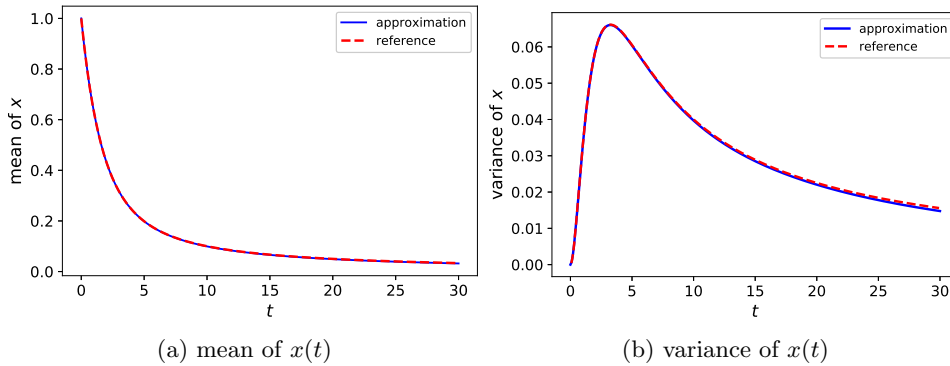


Fig. 5.1: Mean and variance of the solution to Example 1 with $x_0 = 1$.

In Fig. 5.2, we present the propagation of the errors in the mean and the variance. We observe that the error in the mean grows at the beginning and then stays around 10^{-3} after 150 steps of compositions. As for the error in the variance. It grows exponentially with n , which is expected by the error estimate in (4.4).

Example 2: Linear ODE System. Next, let us consider the following ODE system

$$\begin{aligned} \frac{dx_1}{dt} &= x_1 - \alpha_1(\omega)x_2, \\ \frac{dx_2}{dt} &= \alpha_2(\omega)x_1 - 7x_2, \end{aligned} \quad (5.3)$$

with $\alpha = (\alpha_1, \alpha_2) \in I_\alpha = (3.8, 4.2)^2$ and $I_{\mathbf{x}} = [-1, 1]^2$. We use a fully connected block of the structure (3, 40) to construct $\hat{\Phi}_\delta$. After the training is done, we assign uniform distribution to the parameters and use a tensor product of five-point Gaussian quadrature for approximating the mean and variance. In Fig. 5.3, we present the results with $\mathbf{x}_0 = (0, 1)$ and $n = 100$. A good match between the DNN approximation and the reference is observed.

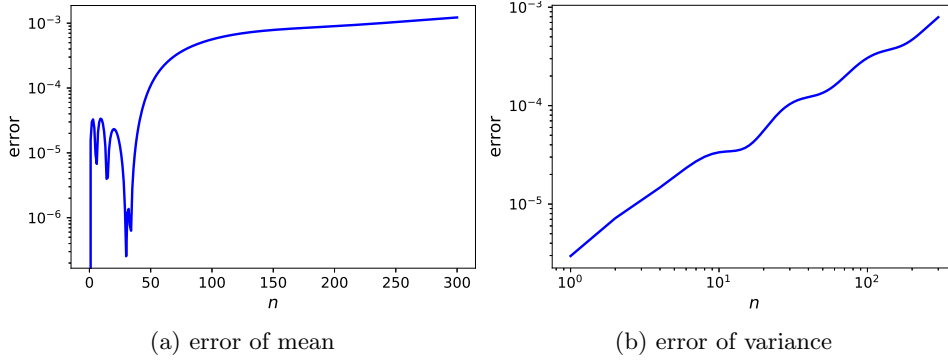


Fig. 5.2: The propagation of errors in mean (left) and variance (right) of the solution to Example 1 with $x_0 = 1$.

Example 3: Nonlinear Random Oscillation. In this example, let us consider the following nonlinear oscillator

$$\begin{aligned} \frac{dx_1}{dt} &= x_2, \\ \frac{dx_2}{dt} &= -\alpha_1(\omega)x_2 - \alpha_2(\omega)\sin x_1. \end{aligned} \quad (5.4)$$

with $\alpha = (\alpha_1, \alpha_2)$ uniformly distributed over the domain $I_\alpha = [0, 0.4] \times [8.8, 9.2]$ and we take $I_x = [-\pi, \pi] \times [-2\pi, 2\pi]$.

The flow map is approximated by a DNN with structure (3, 40). The mean and variance are computed in the same way as in Example 2. In Fig. 5.4, we present the results with $\mathbf{x}_0 = (-1.193, -3.876)$ and $n = 200$. A good performance is observed for the approximation for both the mean and the variance. For the variance approximation, a slight deviation is observed after $t = 12.5$, i.e., $n = 125$. This is due to the accumulation of the error as shown in (4.4). We further plot the propagation of the error of the variance approximation in Fig. 5.5. The error grows slowly with respect to n . The oscillation is due to the oscillatory behavior of the solution.

Example 4: Cell Signaling Cascade. The last example is a mathematical model for autocrine cell-signaling loop developed in [43], which takes the following form.

$$\begin{aligned} \frac{de_{1p}}{dt} &= \frac{I}{1 + Ge_{3p}} \frac{V_{\max,1}(1 - e_{1p})}{K_{m,1} + (1 - e_{1p})} - \frac{V_{\max,2}e_{1p}}{K_{m,2} + e_{1p}}, \\ \frac{de_{2p}}{dt} &= \frac{V_{\max,3}e_{1p}(1 - e_{2p})}{K_{m,3} + (1 - e_{2p})} - \frac{V_{\max,4}e_{2p}}{K_{m,4} + e_{2p}}, \\ \frac{de_{3p}}{dt} &= \frac{V_{\max,5}e_{2p}(1 - e_{3p})}{K_{m,5} + (1 - e_{3p})} - \frac{V_{\max,6}e_{3p}}{K_{m,6} + e_{3p}}. \end{aligned} \quad (5.5)$$

The state variables e_{1p} , e_{2p} , and e_{3p} denote the dimensionless concentrations of the active form of the enzymes. This model contains 13 parameters: $K_{m,1-6}$, $V_{\max,1-6}$, and G , and a tuning parameter I with range $[0, 1.5]$. For the biological meaning of these parameters, see [43].

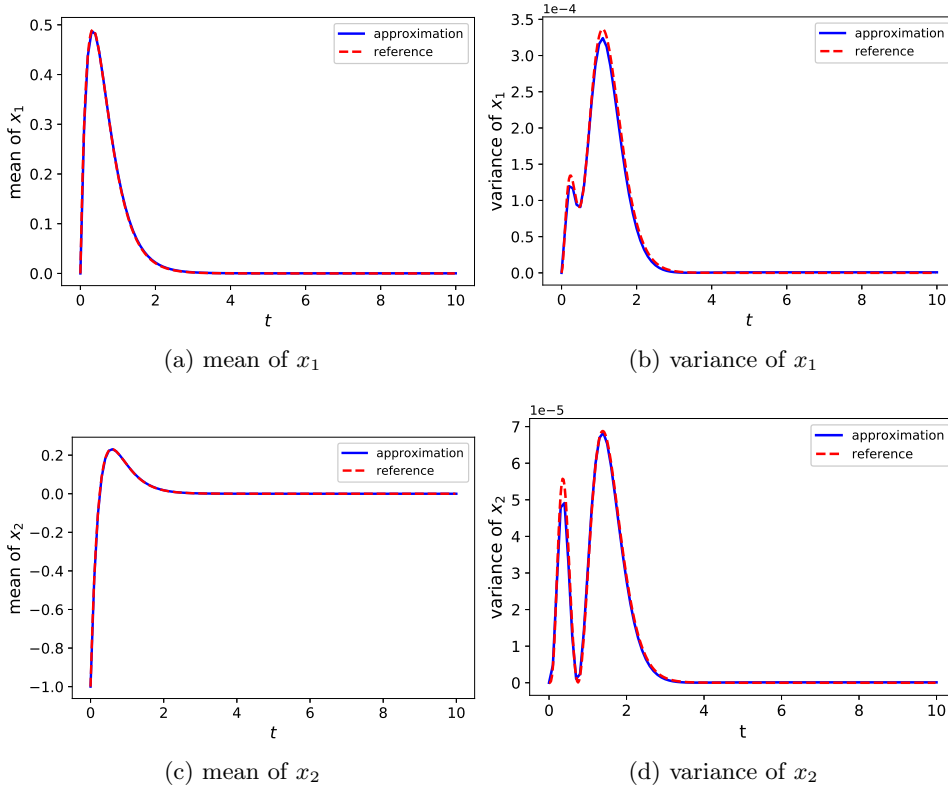


Fig. 5.3: Mean and variance of the solution to Example 2 with $\mathbf{x}_0 = (0, -1)$.

In [43], the parameters take the following values $K_{m,1-6} = 0.2$, $V_{\max,1} = 0.5$, $V_{\max,2} = 0.15$, $V_{\max,3} = 0.15$, $V_{\max,4} = 0.15$, $V_{\max,5} = 0.25$, $V_{\max,6} = 0.05$, and $G = 2$. Here, we introduce 10% relative noise for each parameter and consider the influence on the solution.

Each concentration should fall between 0 and 1 and hence we take $I_{\mathbf{x}} = [0, 1]^3$. Moreover, to ensure the output of the DNN falls in this physical bound, we add an activation function $\sigma_{\text{output}} = \tanh(x)$ on each output node. The fully connected block in the network employed here has a structure with 3 layers and 200 nodes each layer. For illustration purpose, we calculate the mean and variance of the state variables with respect to the random parameters $K_{m,1}$, $K_{m,4}$, $V_{\max,2}$, and $V_{\max,5}$. For other parameters, we assign the noiseless values to them and treat them as deterministic. The tuning parameter I is taken to be 0.48.

After the training is finished, we march forward for $n = 1400$ steps with the initial condition $\mathbf{x}_0 = (0.22685145, 0.98369158, 0.87752945)$ and compute the mean and variance with a tensor product of five-point Gaussian quadrature. In Fig. 5.6, we present the approximated mean and variance. Given such long-time simulation, the approximation agrees well enough with the reference.

For this example, the response curve of e_{3p} with respect to the tuning parameter I is of particular interest in practice. We examine such curve at the steady state of e_{3p} . To this end, we fix all the other parameters at their mean value and let I vary

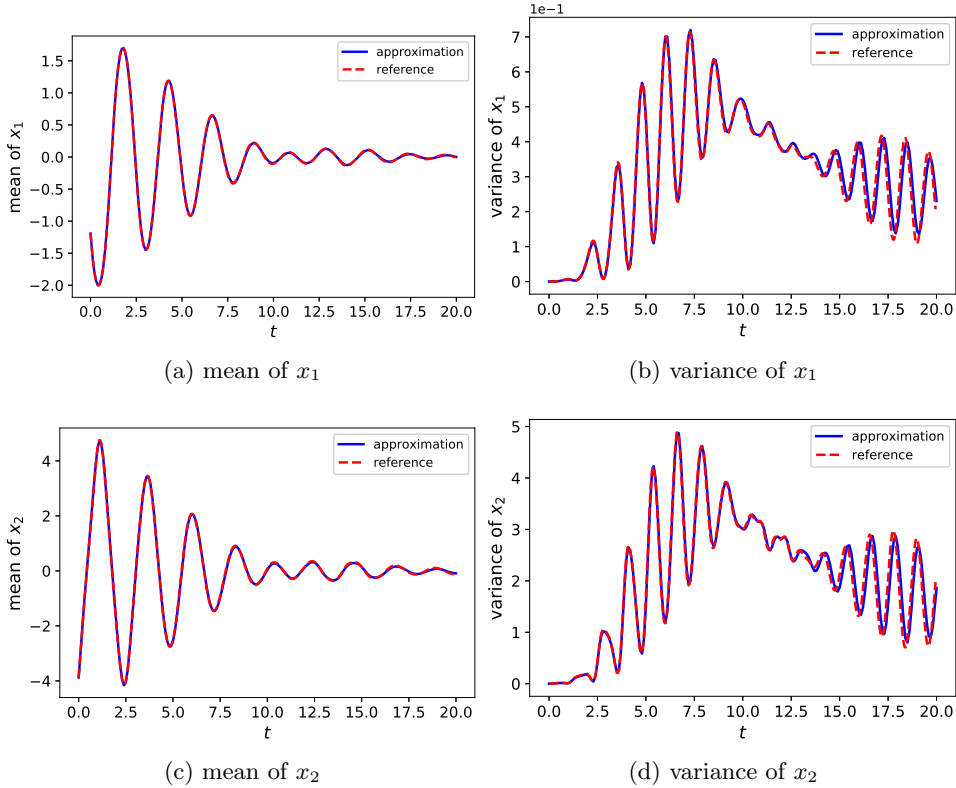
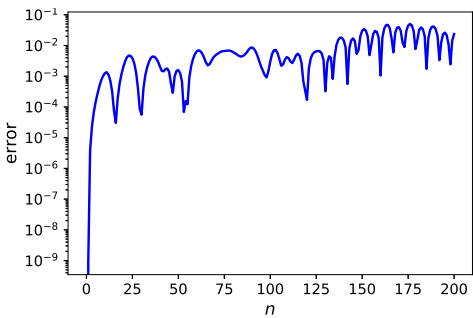


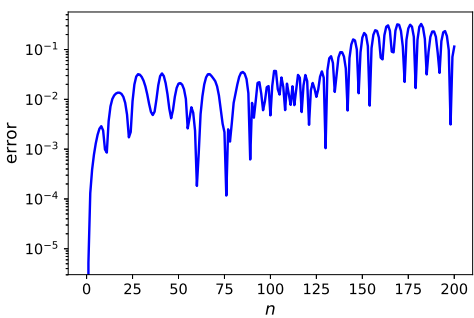
Fig. 5.4: Mean (left column) and variance (right column) of the solution to Example 3 with $x_0 = (-1.193, -3.876)$.

in $[0, 1.5]$. To reach the steady state, without solving the solution for long time, we march the approximated flow map $\hat{\Phi}_\Delta$ forward for 2000 steps. In Fig. 5.7, present the result. A good agreement between the approximation and the reference response curve is observed.

6. Conclusion. We have presented a new approach network for uncertainty quantification basing on the neural network. The neural network is approximating the solution map in the parameter space, of which the dimension is usually very high. The network structure is a modification to the residual network and is mimicking the exact integral form of the flow map. The neural network can be trained off line by using data generated by running high-fidelity numerical solvers or by doing experiment measurements for a short time. Then the trained network can be used as surrogate to compute the statistics of the solution once the distribution of the input random parameters are given.

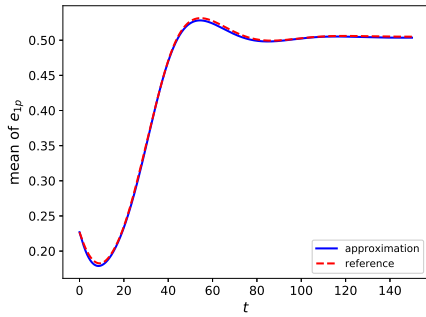


(a) error of variance of x_1

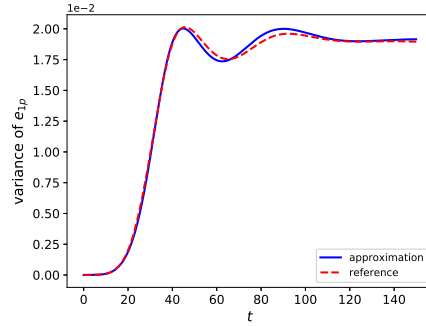


(b) error of variance of x_2

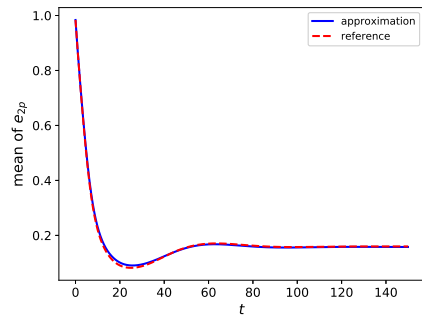
Fig. 5.5: Propagation of errors in the variance of the solution to Example 3 with $x_0 = (-1.193, -3.876)$.



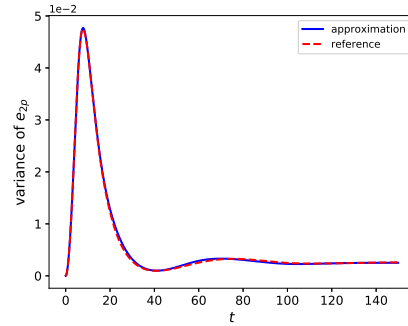
(a) mean of e_{1p}



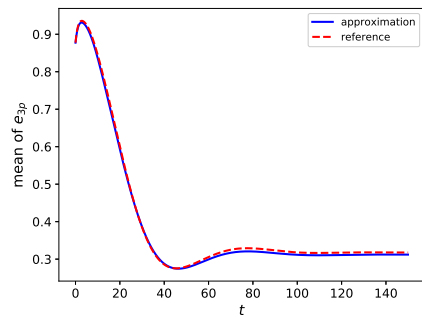
(b) variance of e_{1p}



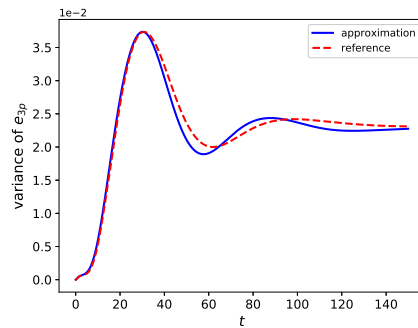
(c) mean of e_{2p}



(d) variance of e_{2p}



(e) mean of e_{3p}



(f) variance of e_{3p}

Fig. 5.6: Mean (left column) and variance (right column) of the solution to Example 4.

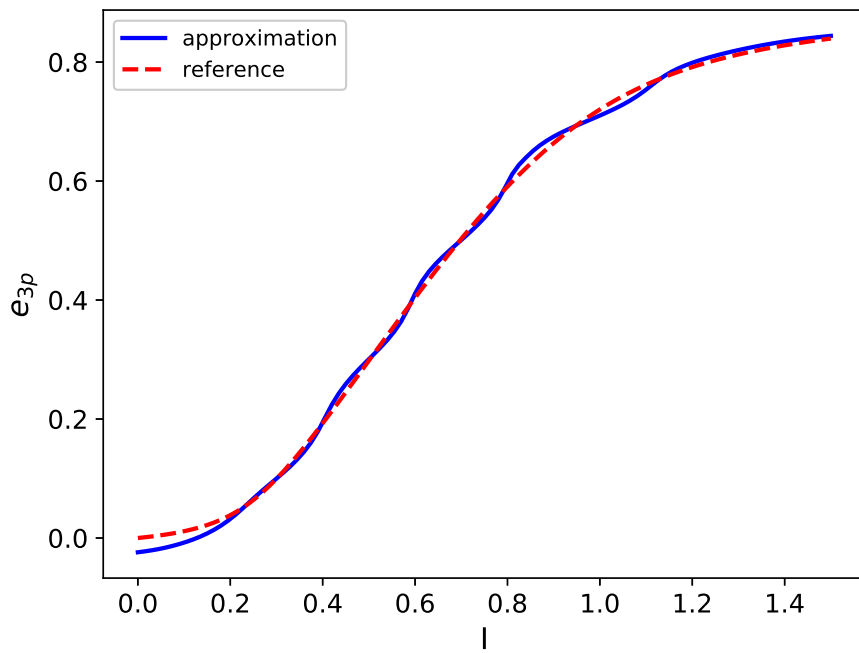


Fig. 5.7: Response curve of the steady state of e_{3p} with respect to I for Example 4.

REFERENCES

- [1] M. ABADI, A. AGARWAL, P. BARHAM, E. BREVDO, Z. CHEN, C. CITRO, G. S. CORRADO, A. DAVIS, J. DEAN, M. DEVIN, S. GHEMAWAT, I. GOODFELLOW, A. HARP, G. IRVING, M. ISARD, Y. JIA, R. JOZEFOWICZ, L. KAISER, M. KUDLUR, J. LEVENBERG, D. MANÉ, R. MONGA, S. MOORE, D. MURRAY, C. OLAH, M. SCHUSTER, J. SHLENS, B. STEINER, I. SUTSKEVER, K. TALWAR, P. TUCKER, V. VANHOUCKE, V. VASUDEVAN, F. VIÉGAS, O. VINYALS, P. WARDEN, M. WATTENBERG, M. WICKE, Y. YU, AND X. ZHENG, *TensorFlow: Large-scale machine learning on heterogeneous systems*, 2015, <https://www.tensorflow.org/>. Software available from tensorflow.org.
- [2] I. BABUSKA, F. NOBILE, AND R. TEMPONE, *A stochastic collocation method for elliptic partial differential equations with random input data*, SIAM Journal on Numerical Analysis, 45 (2007), pp. 1005–1034.
- [3] I. BABUSKA, R. TEMPONE, AND G. E. ZOURARIS, *Galerkin finite element approximations of stochastic elliptic partial differential equations*, SIAM Journal on Numerical Analysis, 42 (2004), pp. 800–825.
- [4] A. R. BARRON, *Universal approximation bounds for superpositions of a sigmoidal function*, IEEE Transactions on Information Theory, 39 (1993), pp. 930–945.
- [5] R. E. BELLMAN, *Adaptive control processes: a guided tour*, vol. 2045, Princeton university press, 2015.
- [6] M. BIANCHINI AND F. SCARSELLI, *On the complexity of neural network classifiers: A comparison between shallow and deep architectures*, IEEE transactions on neural networks and learning systems, 25 (2014), pp. 1553–1565.
- [7] I. BILIONIS AND N. ZABARAS, *Multi-output local gaussian process regression: Applications to uncertainty quantification*, Journal of Computational Physics, 231 (2012), pp. 5718–5746.
- [8] I. BILIONIS, N. ZABARAS, B. A. KONOMI, AND G. LIN, *Multi-output separable gaussian process: Towards an efficient, fully bayesian paradigm for uncertainty quantification*, Journal of Computational Physics, 241 (2013), pp. 212–239.
- [9] S. L. BRUNTON, B. W. BRUNTON, J. L. PROCTOR, E. KAISER, AND J. N. KUTZ, *Chaos as an intermittently forced linear system*, Nature Communications, 8 (2017).
- [10] S. L. BRUNTON, J. L. PROCTOR, AND J. N. KUTZ, *Discovering governing equations from data by sparse identification of nonlinear dynamical systems*, Proc. Natl. Acad. Sci. U.S.A., 113 (2016), pp. 3932–3937.
- [11] R. T. Q. CHEN, Y. RUBANOVA, J. BETTENCOURT, AND D. DUVENAUD, *Neural ordinary differential equations*, arXiv preprint arXiv:1806.07366, (2018).
- [12] X. CHEN, E.-J. PARK, AND D. XIU, *A flexible numerical approach for quantification of epistemic uncertainty*, Journal of Computational Physics, 240 (2013), pp. 211–224.
- [13] P. G. CONSTANTINE, E. DOW, AND Q. WANG, *Active subspace methods in theory and practice: applications to kriging surfaces*, SIAM Journal on Scientific Computing, 36 (2014), pp. A1500–A1524.
- [14] K.-L. DU AND M. SWAMY, *Neural networks and statistical learning*, Springer-Verlag, 2014.
- [15] R. ELKAN AND O. SHAMIR, *The power of depth for feedforward neural networks*, in Conference on Learning Theory, 2016, pp. 907–940.
- [16] M. S. ELDRED, L. P. SWILER, AND G. TANG, *Mixed aleatory-epistemic uncertainty quantification with stochastic expansions and optimization-based interval estimation*, Reliability Engineering & System Safety, 96 (2011), pp. 1092–1113.
- [17] M. GERRITSMA, J.-B. VAN DER STEEN, P. VOS, AND G. KARNIADAKIS, *Time-dependent generalized polynomial chaos*, Journal of Computational Physics, 229 (2010), pp. 8333–8363.
- [18] R. GHANEM AND P. D. SPANOS, *Polynomial chaos in stochastic finite elements*, Journal of Applied Mechanics, 57 (1990), pp. 197–202.
- [19] I. GOODFELLOW, Y. BENGIO, AND A. COURVILLE, *Deep learning*, MIT Press, 2016.
- [20] K. HE, X. ZHANG, S. REN, AND J. SUN, *Deep residual learning for image recognition*, in Proceedings of the IEEE conference on computer vision and pattern recognition, 2016, pp. 770–778.
- [21] J. HELTON, J. JOHNSON, W. OBERKAMPF, AND C. B. STORLIE, *A sampling-based computational strategy for the representation of epistemic uncertainty in model predictions with evidence theory*, Computer Methods in Applied Mechanics and Engineering, 196 (2007), pp. 3980–3998.
- [22] J. C. HELTON, J. D. JOHNSON, W. L. OBERKAMPF, AND C. J. SALLABERRY, *Representation of analysis results involving aleatory and epistemic uncertainty*, International Journal of General Systems, 39 (2010), pp. 605–646.
- [23] J. HESTHAVEN AND S. UBBIALI, *Non-intrusive reduced order modeling of nonlinear problems*

- using neural networks, *J. Comput. Phys.*, 363 (2018), pp. 55–78.
- [24] G. HINTON, L. DENG, D. YU, G. E. DAHL, A.-R. MOHAMED, N. JAITLEY, A. SENIOR, V. VANHOUCHE, P. NGUYEN, T. N. SAINATH, ET AL., *Deep neural networks for acoustic modeling in speech recognition: The shared views of four research groups*, *IEEE Signal Processing Magazine*, 29 (2012), pp. 82–97.
- [25] K. HORNIK, *Approximation capabilities of multilayer feedforward networks*, *Neural Networks*, 4 (1991), pp. 251–257.
- [26] J. JAKEMAN, M. ELDERED, AND D. XIU, *Numerical approach for quantification of epistemic uncertainty*, *Journal of Computational Physics*, 229 (2010), pp. 4648–4663.
- [27] D. P. KINGMA AND J. BA, *Adam: A method for stochastic optimization*, arXiv preprint arXiv:1412.6980, (2014).
- [28] A. KRIZHEVSKY, I. SUTSKEVER, AND G. E. HINTON, *Imagenet classification with deep convolutional neural networks*, in *Advances in neural information processing systems*, 2012, pp. 1097–1105.
- [29] I. E. LAGARIS, A. LIKAS, AND D. I. FOTIADIS, *Artificial neural networks for solving ordinary and partial differential equations*, *IEEE transactions on neural networks*, 9 (1998), pp. 987–1000.
- [30] S. LIANG AND R. SRIKANT, *Why deep neural networks for function approximation?*, arXiv preprint arXiv:1610.04161, (2016).
- [31] Z. LONG, Y. LU, X. MA, AND B. DONG, *PDE-Net: learning PDEs from data*, arXiv preprint arXiv:1710.09668, (2017).
- [32] X. MA AND N. ZABARAS, *An adaptive hierarchical sparse grid collocation algorithm for the solution of stochastic differential equations*, *Journal of Computational Physics*, 228 (2009), pp. 3084–3113.
- [33] A. MARDT, L. PASQUALI, H. WU, AND F. NOE, *VAMPnets for deep learning of molecular kinetics*, *Nature Comm.*, 9 (2018), p. 5.
- [34] G. F. MONTUFAR, R. PASCANU, K. CHO, AND Y. BENGIO, *On the number of linear regions of deep neural networks*, in *Advances in neural information processing systems*, 2014, pp. 2924–2932.
- [35] A. PINKUS, *Approximation theory of the MLP model in neural networks*, *Acta Numerica*, 8 (1999), pp. 143–195.
- [36] T. POGGIO, H. MHASKAR, L. ROSASCO, B. MIRANDA, AND Q. LIAO, *Why and when can deep-but not shallow-networks avoid the curse of dimensionality: A review*, *International Journal of Automation and Computing*, 14 (2017), pp. 503–519.
- [37] T. QIN, K. WU, AND D. XIU, *Data driven governing equations approximation using deep neural networks*, *Journal of Computational Physics*, (2019).
- [38] M. RAISSI, *Deep hidden physics models: Deep learning of nonlinear partial differential equations*, *The Journal of Machine Learning Research*, 19 (2018), pp. 932–955.
- [39] D. RAY AND J. HESTHAVEN, *An artificial neural network as a troubled-cell indicator*, *J. Comput. Phys.*, 367 (2018), pp. 166–191.
- [40] D. RAY AND J. S. HESTHAVEN, *Detecting troubled-cells on two-dimensional unstructured grids using a neural network*, *Journal of Computational Physics*, 397 (2019), p. 108845.
- [41] S. H. RUDY, J. N. KUTZ, AND S. L. BRUNTON, *Deep learning of dynamics and signal-noise decomposition with time-stepping constraints*, *Journal of Computational Physics*, 396 (2019), pp. 483–506.
- [42] J. SCHMIDHUBER, *Deep learning in neural networks: an overview*, *Neural Networks*, 61 (2015), pp. 85–117.
- [43] S. Y. SHVARTSMAN, M. HAGAN, A. YACCOUB, P. DENT, H. WILEY, AND D. A. LAUFFENBURGER, *Autocrine loops with positive feedback enable context-dependent cell signaling*, *American Journal of Physiology-Cell Physiology*, 282 (2002), pp. C545–C559.
- [44] D. SILVER, A. HUANG, C. J. MADDISON, A. GUEZ, L. SIFRE, G. VAN DEN DRIESSCHE, J. SCHRIETWIESER, I. ANTONOGLU, V. PANNEERSHELVAM, M. LANCTOT, ET AL., *Mastering the game of go with deep neural networks and tree search*, *nature*, 529 (2016), pp. 484–489.
- [45] S. A. SMOLYAK, *Quadrature and interpolation formulas for tensor products of certain classes of functions*, in *Doklady Akademii Nauk*, vol. 148, Russian Academy of Sciences, 1963, pp. 1042–1045.
- [46] A. STUART AND A. R. HUMPHRIES, *Dynamical Systems and Numerical Analysis*, vol. 2, Cambridge University Press, 1998.
- [47] R. K. TRIPATHY AND I. BILIONIS, *Deep uq: Learning deep neural network surrogate models for high dimensional uncertainty quantification*, *Journal of Computational Physics*, 375 (2018), pp. 565–588.
- [48] E. WEINAN AND B. YU, *The deep ritz method: a deep learning-based numerical algorithm for*

- solving variational problems*, Communications in Mathematics and Statistics, 6 (2018), pp. 1–12.
- [49] K. WU AND D. XIU, *Numerical aspects for approximating governing equations using data*, J. Comput. Phys., in press (2019).
- [50] D. XIU, *Efficient collocational approach for parametric uncertainty analysis*, Communications in computational physics, 2 (2007), pp. 293–309.
- [51] D. XIU AND J. S. HESTHAVEN, *High-order collocation methods for differential equations with random inputs*, SIAM Journal on Scientific Computing, 27 (2005), pp. 1118–1139.
- [52] D. XIU AND G. E. KARNIAKAKIS, *The wiener–askey polynomial chaos for stochastic differential equations*, SIAM journal on scientific computing, 24 (2002), pp. 619–644.
- [53] Y. YANG AND P. PERDIKARIS, *Adversarial uncertainty quantification in physics-informed neural networks*, Journal of Computational Physics, 394 (2019), pp. 136–152.
- [54] Y. ZHU AND N. ZABARAS, *Bayesian deep convolutional encoder–decoder networks for surrogate modeling and uncertainty quantification*, Journal of Computational Physics, 366 (2018), pp. 415–447.
- [55] Y. ZHU, N. ZABARAS, P.-S. KOUTSOURELAKIS, AND P. PERDIKARIS, *Physics-constrained deep learning for high-dimensional surrogate modeling and uncertainty quantification without labeled data*, Journal of Computational Physics, 394 (2019), pp. 56–81.